Visualization of Mucosal Vasculature with Narrow Band Imaging: A Theoretical Study

Quanzeng Wang[1*†], Du Le[1,2†], Jessica Ramella-Roman[2] and Joshua Pfefer[1]

[1]Center for Devices & Radiological Health, Food and Drug Administration, Silver Spring, MD 20993, USA
[2] Department of Biomedical Engineering, Catholic University of America, Washington, DC 20064, USA
quanzeng.wang@fda.hhs.gov; † These authors contributed equally

ABSTRACT

Narrow band imaging (NBI) is a spectrally-selective reflectance imaging technique that is used as an adjunctive approach to endoscopic detection of mucosal abnormalities such as neoplastic lesions. While numerous clinical studies in tissue sites such as the esophagus, oral cavity and lung indicate the efficacy of this approach, it is not well theoretically understood. In this study, we performed Monte Carlo simulations to elucidate the factors that affect NBI device performance. The model geometry involved a two-layer turbid medium based on mucosal tissue optical properties and embedded cylindrical, blood-filled vessels at varying diameters and depths. Specifically, we studied the effect of bandpass filters (415±15 nm, 540±10 nm versus white light), blood vessel diameter (20-400 μm) and depth (30 - 450 μm), wavelength, and bandwidth on vessel contrast. Our results provide a quantitative evaluation of the two mechanisms that are commonly believed to be the primary components of NBI: (i) the increased contrast provided by high hemoglobin absorption and (ii) increase in the penetration depth produced by the decrease in scattering with increasing wavelength. Our MC model can provide novel, quantitative insight into NBI, may lead to improvements in its performance.

Keywords: Narrow band imaging, Monte Carlo modeling, reflectance, light-tissue interaction, mucosal cancer

1. INTRODUCTION

Mucosal cancers arising in oral cavity, pharynx, and digestive system are responsible for nearly 140,000 deaths annually in the US[1], thus representing a major public concern. It is reported that the invasion of tumors into submucosal layers is associated with the increasing of microvessel density and intrapapillary capillary loops (IPCLs) can become less transparent than the normal mucosa and more dilated and elongated, causing roughness in the vessels surface at later stages of carcinoma [2]. Pathological study has shown that intratumoral microvessel density increases in proportion to the progression of esophageal Barrett's-associated adenocarcinoma [3]. Therefore, good visualizations of vasculature may provide useful information for early detection of mucosal cancer.

Many clinical studies have indicated that narrow band imaging (NBI) has the potential to improve detection of mucosal neoplasia. Sharma *et al.* [4] used a NBI system associated with magnifying endoscopy to evaluate microvessel features of esophagus, thus providing valuable optical data for diagnosis of patients with Barrett's esophagus. A similar NBI system was also used to distinguish types of IPCLs for early detection of oral neoplastic lesions by Takano *et al.* [5], of superficial esophageal lesions by Yoshida *et al.* [6], of gastroesophageal reflux disease by Ishihara *et al.* [7] and Sharma *et al.* [8].

Furthermore, NBI was reported as a promising technique in predicting the invasion depth of early colorectal cancer in mucosa [9-11]. The NBI system used in these studies has a common set of optical filters with centre wavelengths at 415, 445, and 500 nm (bandwidth of 30 nm for each filters) which were selected to enhance the visualization of capillary vessels and were estimated to have penetration depths of 170 μm, 200 μm and 240 μm, respectively [6, 12]. This filter set was proposed as the first trial case for clinical tests in Gono's study which classified mucosal patterns into three classes with diameters ranging from 10 to 500 μm and explained the changes in image contrast of each class as due to tissue and blood absorption and scattering [13]. In addition, narrow band filters with center wavelengths of 415 nm (bandwidth 30 nm) and 540 nm (bandwidth 10 nm) have been used to enhance mucosal capillary patterns [14], to diagnose biliary-tract diseases [15], and to image colon cancer *in vivo* [16]. Previous studies also reported that superior visualization of small vessels (diameter 10 to 20 μm) at shallow depth can be obtained with narrow band filters having center wavelength at 415 nm [13].

Design and Quality for Biomedical Technologies V, edited by Ramesh Raghavachari, Rongguang Liang,
Proc. of SPIE Vol. 8215, 821505 · © 2012 SPIE · CCC code: 1605-7422/12/$18 · doi: 10.1117/12.906817

The basic theory of NBI is based on hemoglobin (Hb) absorption and tissue scattering. Hb has absorption peaks in blue (415 nm) and green (540 nm) regions of the spectrum while mucosal scattering decays monotonically with wavelength. Thus, 415 nm can be used to visualize thin mucosal vasculature in superficial regions while 540 nm can be used to visualize thicker vessels at deeper regions. Image contrast in NBI techniques have been quantified in various study [6, 17]. In a study to distinguish IPCL from background mucosal, Yoshida *et al*. showed that image contrast of narrowband illumination was superior to that of conventional broadband illumination, and that contrast reached maximum (0.96±0.31) when blue filter was used. Using only green filter (540±10 nm) and broadband light in visualizing blood vessels in laparoscopic surgery on a pig, Akabari *et al*. also showed that image contrast strongly improved (with absolute difference of 0.18) when using green filter [17].

While the basic mechanisms of NBI appear to have been established, a quantitative understanding of the effect of tissue and device parameters has not been achieved. In this study, we have developed and implemented Monte Carlo (MC) algorithms to calculate contrast as a function of vessels depth and diameter, with a focus on 415±15 nm, 540±10 nm and white (400-650 nm) light. This was accomplished by incorporating mucosal layered tissues and vessel-like structures into a three-dimensional (3-D), voxel-based MC model [18]. In addition, the effect of wavelength and bandwidth on image contrast was investigated.

Voxel-based MC algorithms have been developed to represent complex media by Pfefer *et al* [18] and applied to selective photothermolysis of port wine stains. This approach can reproduce arbitrary 3-D heterogenous structures such as skin comprised of epidermis, dermis and blood vessels. Subsequent work has applied 3-D MC models to applications such as brain and bone imaging [19, 20]. However, visualization of vasculature with NBI has not been addressed with MC or other advanced numerical modeling approaches.

2. METHODS

2.1 Representation of mucosal tissue morphology

Since most mucosal tissues have two layers, epithelium and stroma, with distinguished optical properties (OPs) of absorption coefficient (μ_a) and reduced scattering coefficient (μ_s') [21, 22], a material grid array was generated to specify the geometries of tissue-simulating media. Each integer in the array represented a voxel corresponding to a material – epithelium, stroma or blood vessel. An example of a material grid is shown in Fig. 1. The number of voxels in x, y and z directions was 140, 140 and 100, respectively. The size of each voxel was 10 μm in each direction. Thus, the tissue-simulating medium used in each simulation had dimension of 1.4 mm x 1.4 mm x 1.0 mm. The thickness of epithelium was 30 μm and that of stroma was 970 μm. A single cylindrical blood vessel was located in the stroma layer in y direction and was symmetric in x direction. The vessel diameter ranged from 20 to 400 μm, corresponding to those found in mucosal tissues [13]. Vessel depth was defined as the distance from the top surface of the epithelium to the vessel's top boundary, and ranged from 30 to 450 μm. Each simulation was performed using 300 million photons. The 3-D voxel-based MC simulations of photon propagation are described in detail elsewhere [18].

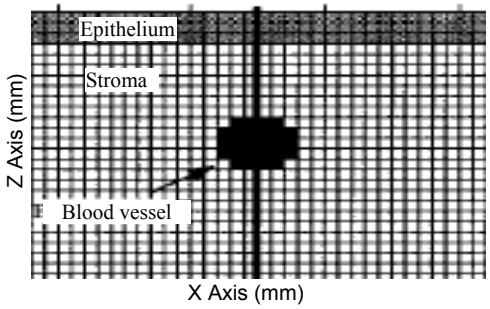

Fig. 1 Voxel-based grid geometry of a tissue-simulating medium in the x-z plane

2.2 OPs of mucosal tissues and of human blood

The tissue-simulating media had two different layers with unique, spectrally varying OPs of epithelium (μ_{a1} and μ_{s1}') and stroma (μ_{a2} and μ_{s2}'). OPs of epithelium and μ_{s2}' were extracted from prior work by Drezek *et al*. [21]. As for μ_{a2}, absorption was assumed to be due to two constituents: Hb and collagen [22]. OPs of human blood (μ_{a0} and μ_{s0}') are mainly determined by two factors: Hb concentration and hematocrit level [23]. The normal Hb concentration for adults ranges from 11.5 to 13.7 *g*/dL [24] and the normal hematocrit level in adult blood ranges from 36% to 47% [25]. In this study, the OPs of blood were extracted from Friebel *et al.*'s studies with the Hb concentration set as 12.9 *g*/dL, and the hematocrit set as 42.1% [23]. In addition, Hb was assumed to be fully oxygenated. Similar human blood OPs were also described elsewhere[26]. The OPs used in this study are displayed graphically in Fig. 2.

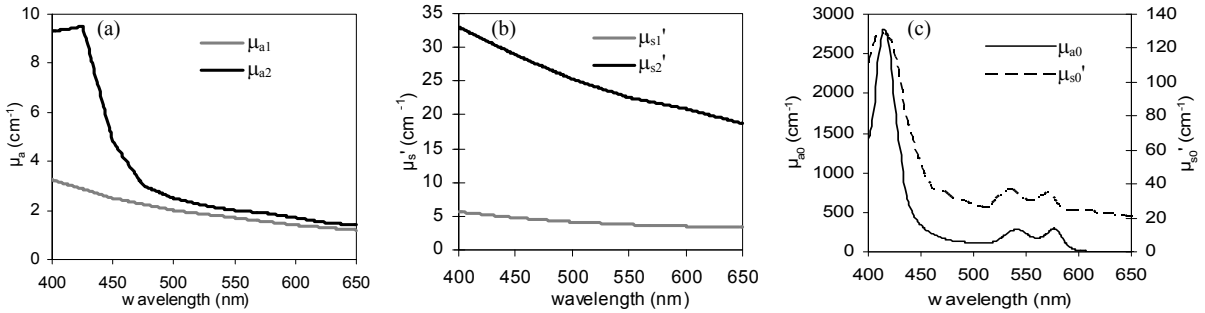

Fig. 2 OPs of (a, b) mucosal tissues and (c) oxygenated human blood

2.3 Contrast calculation

The direct results of a 3-D voxel-based MC simulation was a reflectance image in the *x*-*y* plane on the top surface of the tissue-simulating medium (Fig. 3a). The image was quantified with contrast that was calculated as $Contrast=(I_b-I_v)/I_b$, where I_b is intensity of background area and I_v is intensity of blood vessel area (Fig. 3b). This method was based on Weber's law that had been applied in different NBI studies [13][27]. Since blood is the dominated tissue absorber in the ultraviolet-visible range, I_b is larger than I_v. Thus, it is most likely that contrast has a positive value. In this study, contrast was a dependent variable that was expressed as a function of vessel size, vessel depth, wavelength, and bandwidth of illumination spectra.

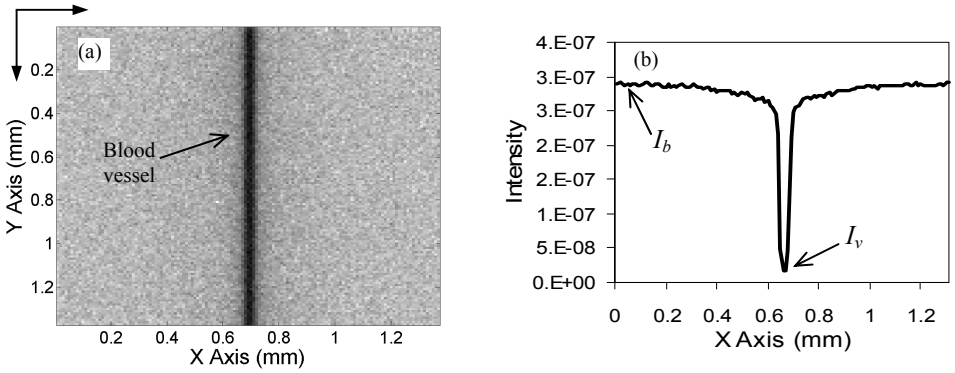

Fig. 3 (a) Reflectance image in *x*-*y* plane from a 3-D voxel-based MC simulation and (b) its contrast calculation in the *x* direction

2.4 Illumination spectra and weighting of OPs for single-simulation method

Fig. 4 shows the illumination spectra of conventional white light system (Fig. 4a) and of a NBI system with bandpass filters of 415±15 nm (Fig. 4b) and 540±10 nm (Fig. 4c) from journal papers[28, 29]. In order to perform fast MC simulations over a specific bandwidth, OPs were weighed to the normalized illumination spectra over the whole bandwidth. The intensity-normalized sum of weighted OPs was used to obtain the reflectance image from the whole bandwidth through a single MC simulation. We called this method as single-simulation method. An example of

weighting OPs to normalized illumination spectra is shown in Fig. 5. Table 1 shows weighted OPs for 415±15 and 540±10 nm bands and for white light of 400-650 nm. Each set of OPs were used to simulate reflection distribution over accordingly bandwidth.

Although the single-simulation method reduced simulation time by using the weighted OPs for a single MC simulation over a bandwidth, the idea need to be validated with multi-simulation method. In the multi-simulation method, one MC simulation was performed every 5 nm with the average OPs within the 5 nm range as inputs. Each MC simulation would generate a reflectance image. All the reflectance images within the whole bandwidth were weighted with the normalized illumination spectrum and summed to get the final reflectance image. The contrast of the final reflectance image from the multi-simulation method was used as a standard to evaluate the single-simulation method.

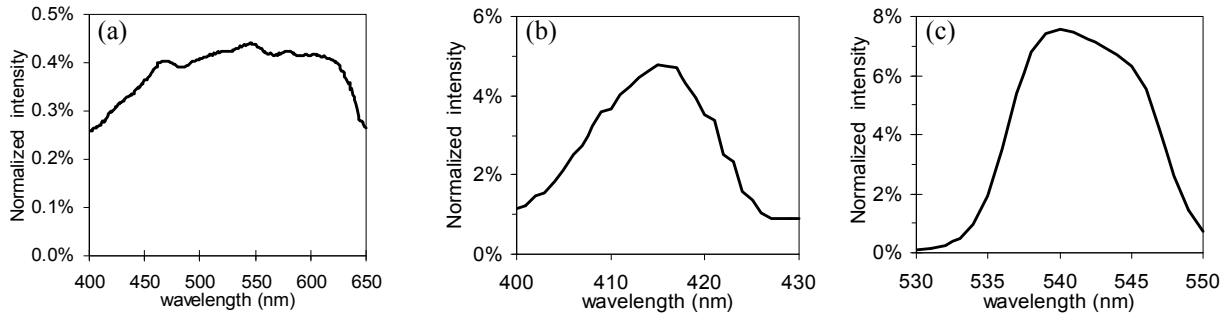

Fig. 4 Illumination spectra of (a) white light, and of filters with center wavelength at (b) 415 nm, (c) 540 nm

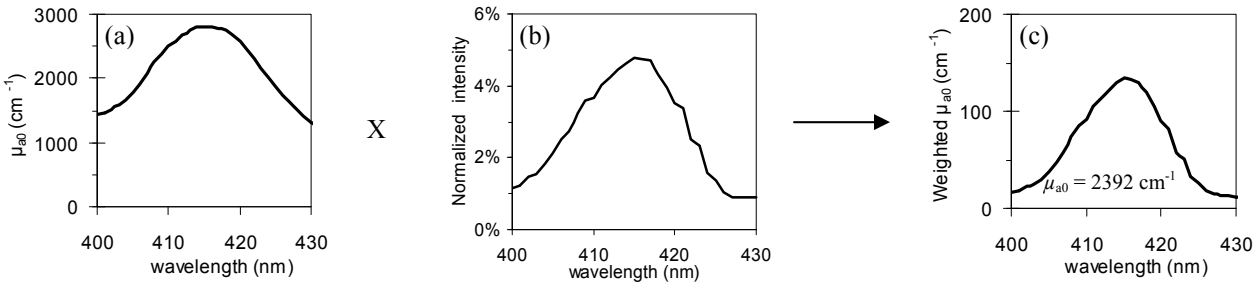

Fig. 5 Weighting OP spectrum with normalized illumination spectrum of 415±15 nm bandpass filter

Table 1. Averaged OPs for 415±15 and 540±10 nm banfpass filters and for 400-650 nm white light source

Bandwidth (nm)	μ_{a1} (cm^{-1})	μ_{s1}' (cm^{-1})	μ_{a2} (cm^{-1})	μ_{s2}' (cm^{-1})	μ_{a0} (cm^{-1})	μ_{s0}' (cm^{-1})
415±15	3.0	5.4	9.4	31.8	2392.6	124.3
540±10	1.8	3.8	2.1	23.0	274.6	33.7
400 - 650	1.9	4.1	3.2	24.4	356.6	40.6

3. RESULTS

3.1 Validation of the single-simulation method with the multi-simulation method

Error! Reference source not found. Table 2 compares contrast values from the single-simulation method with those from the multi-simulation method. Results are presented for NBI bands of 415±15 and 540±10 nm and white light of 400-650 nm for vessel diameters of 50 and 100 μm. As shown from the table, 14 out of 20 cases for the 415±15 and 540±10 nm bands had contrast difference of no more than 1% between the single- and multi-simulation methods. One exception of the 415±15 nm band cases was for the 100 μm diameter vessel at depth of 450 μm, which shows 18.8% contrast difference between the single- and multi-simulation methods. That was because the contrast values from both methods were low and the noise level was high. The results indicate that the single-simulation method was accurate to calculate the contrast for the 415±15 and 540±10 nm bands. However, the percentage difference of contrast values for between the single- and multi-simulation methods ranges from 52.9% to 85.5 when white light was used, indicating that multi-simulation method should be used to accurately simulate white light reflection. Therefore, all the data provided for

narrow band simulations were from the single-simulation method and those for 400-650 nm white light simulations were from the multi-simulation method unless specified.

Table 2. Comparison of contrast values from the single-simulation method with those from the multi-simulation method

		50 μm diameter vessel					100 μm diameter vessel				
Vessel depth (μm)		25	75	125	175	225	50	150	250	350	450
415±15 nm band	Single-simulation	0.941	0.712	0.419	0.240	0.140	0.898	0.461	0.179	0.071	0.034
	Multi-simulation	0.940	0.715	0.422	0.237	0.144	0.896	0.460	0.183	0.070	0.029
	% difference	**0.1%**	**0.4%**	**0.7%**	**0.9%**	**3.2%**	**0.2%**	**0.2%**	**2.2%**	**2.1%**	**18.8%**
540±10 nm band	Single-simulation	0.655	0.524	0.340	0.220	0.143	0.861	0.541	0.272	0.137	0.063
	Multi-simulation	0.653	0.523	0.348	0.221	0.143	0.860	0.536	0.269	0.134	0.063
	% difference	**0.3%**	**0.1%**	**2.4%**	**0.4%**	**0.2%**	**0.1%**	**1.0%**	**1.0%**	**2.0%**	**0.2%**
400-650 nm	Single-simulation	0.739	0.584	0.382	0.238	0.158	0.885	0.535	0.264	0.124	0.058
	Multi-simulation	0.413	0.327	0.212	0.132	0.085	0.579	0.343	0.167	0.079	0.037
	% difference	**79.0%**	**78.8%**	**80.6%**	**79.4%**	**85.5%**	**52.9%**	**55.9%**	**58.5%**	**58.4%**	**55.1%**

3.2 Contrast as a function of vessel diameter and depth

Fig. 6 shows contrast as a function of vessel depth for vessel diameters of 20, 50, 75, 100, 200 and 400 μm (Fig. 6 a-f respectively) when 415±15 nm and 540±10 nm band-pass filters (Fig. 6a-f) and 400-650 nm white light (Fig. 6 b, d and e) were used. In general, as vessel depth increased, contrast decreased. This was because the penetration depth of photons is limited by scattering so as blood vessel depth increased, the probability of a photon being absorbed by the vessel decreased.

For small vessels at superficial depths (diameters of 20, 50 μm, depths of 30-250 μm), the 415 nm band produced higher contrast than the 540 nm band (Fig. 6a, b). This was because blood absorption at 415 nm is significantly higher than that at 540 nm. On the other hand, for larger vessels in deeper regions (diameters of 75-400 μm, depths of 150-450 μm), the reverse was seen. This was because tissue scattering was also crucial in determining contrast. As shown in Fig. 2b and Table 1, tissue scattering was lower at 540 nm than 415 nm. Therefore, the probability for a photon to reach a blood vessel and return to the surface was higher when using illumination at 540 nm region. As a result, the contrast at 415 nm decreased faster with depth than that at 540 nm. An illustration of the relative contrast at 415 and 540 nm was seen for a vessel diameter of 75 μm (Fig. 6c), which showed that, compared with 540 nm illumination, the 415 nm produced higher contrast for depths less than 125 μm and lower contrast for depths greater than 125 μm.

Our results indicate that 540 nm always had better contrast than white light (Fig. 6 b, d, e). The 415 nm band had better contrast than white light for smaller and shallower vessels, but a little worse contrast for larger and deeper vessels. That was because the longer wavelength region of the white light was less scattered than the 415 nm and could penetrate deeper. For a vessel diameter of 100 μm (Fig. 6d), the 415 nm band increased contrast by 55% at 50 μm depth and the 540 nm band increased contrast by 68% at 350 μm depth compared to white light.

Fig. 7 shows the same data as Fig. 6, but with curves grouped by wavelength. This figure indicates that for any given vessel depth, diameter had less effect on contrast for 415 nm than for 540 nm. The difference between the two wavelengths was most evident at shallow depths. The lack of change in contrast for 415 nm was due to the high Hb absorption which causes even small vessels to absorb nearly all the photons reaching them. At 540 nm, larger vessel path length was required to attenuate the vast majority of photons passing through the vessel. Thus, small vessels were difficult to visualize at this wavelength, even at shallow depths. Fig. 7 also indicates that the change in contrast as a function of depth (slope of the curves) tended to decrease with increasing vessel size for 415 nm, whereas 540 nm showed little change.

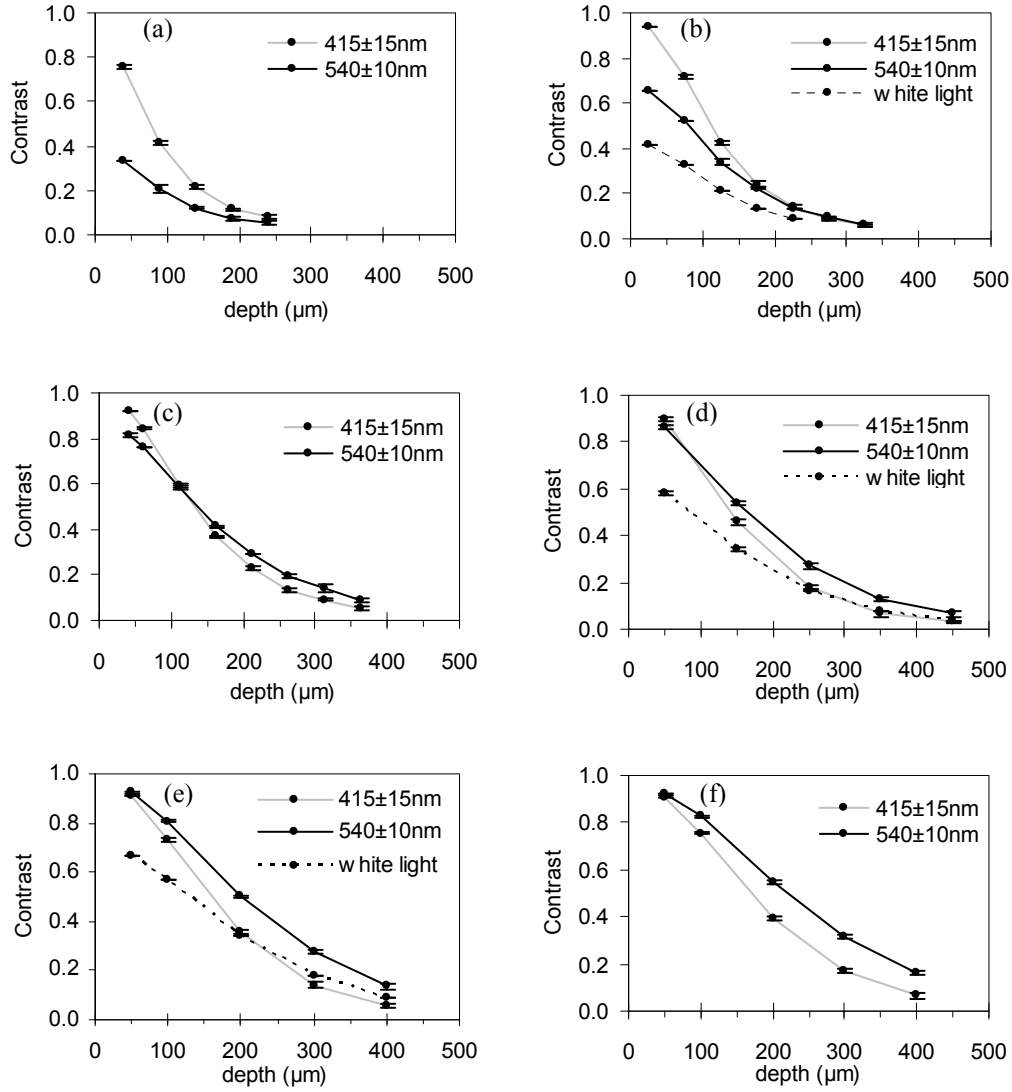

Fig. 6 Contrast as function of vessel depth for vessel diameters of (a) 20, (b) 50, (c) 75, (d) 100, (e) 200, and (f) 400 μm using 415±15, 540±10, and 400-650 nm illuminations

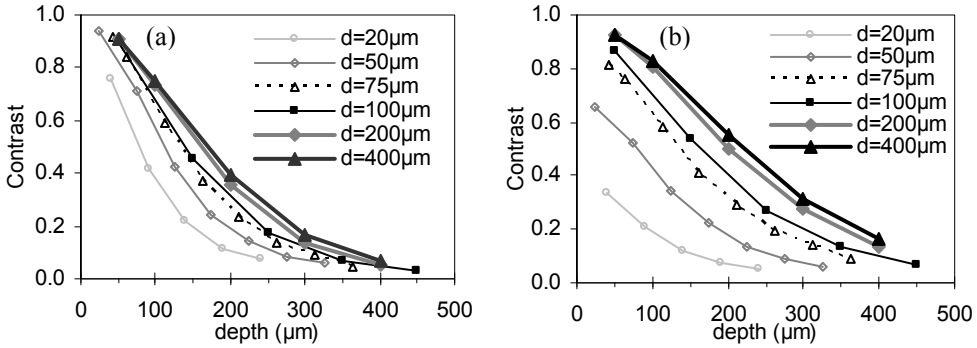

Fig. 7 Contrast versus vessel depth at different vessel diameters (*d*) for (a) 415 ±15, and (b) 540 ± 10 nm illuminations

3.3 Contrast as a function of wavelength and bandwidth

We further investigated the relationship between contrast and wavelength for vessels with diameters of 50 and 100 μm at different depths within the wavelength range of 400-650 nm by performing simulations at 5 nm intervals (Fig. 8). Results indicate that contrast was dominated by competing effects of Hb absorption and tissue scattering; the former acted to increase contrast and the latter to degrade it. The relative impact of each of these two factors depended on vessel size and depth. In Fig. 8a, the peak values of contrast located at 415, 540 and 575 nm concurred with the absorption peaks of Hb, showing the essential effect of Hb absorption on contrast improvement. These graphs indicate that as depth increased, contrast decreased faster at shorter wavelengths because of the higher scattering coefficients.

However, the ratio between Hb absorption coefficients at 415 and 540 nm is 8.7, whereas, in Fig. 8a, the maximum ratio was 1.5. The graph demonstrated why the 575±15 nm band was also used in a prior NBI study [30]. From Fig. 8b, there was also a small peak at the depth of 150 μm for a 100 μm diameter vessel. This might be a reason why the 445 nm band was used [31]. For the 50 μm diameter vessel, 415 nm generated significantly higher contrast than 540 nm for depths less than 125 μm. On the other side, 540 nm showed higher contrast than 415 nm for the 100 μm diameter vessel at depths of more than 150 μm. Since different tissues have different morphologies, it might be possible to identify optimal wavelength bands on the basis of vessel size and depth.

The effect of bandwidth on image contrast was also evaluated for a 50 μm diameter vessel at 415 nm and 540 nm regions (Fig. 9), based on contrast values from the data in Fig. 8a. At 415 nm, contrast was not affected by illumination bandwidth (1.4% reduction for 30 nm bandwidth and 125 μm depth). On the other hand, at 540 nm contrast decreased with illumination bandwidth at all vessel depths (21.1% reduction for 30 nm bandwidth and 125 μm depth). This was because Hb absorption near 415 nm is so high that moderate changes in absorption still presented a condition where photon absorption was extremely strong in blood vessels. However, for 540±15 nm, the lower Hb absorption at wavelengths above and below 540 nm resulted in reduced contrast with increasing bandwidth.

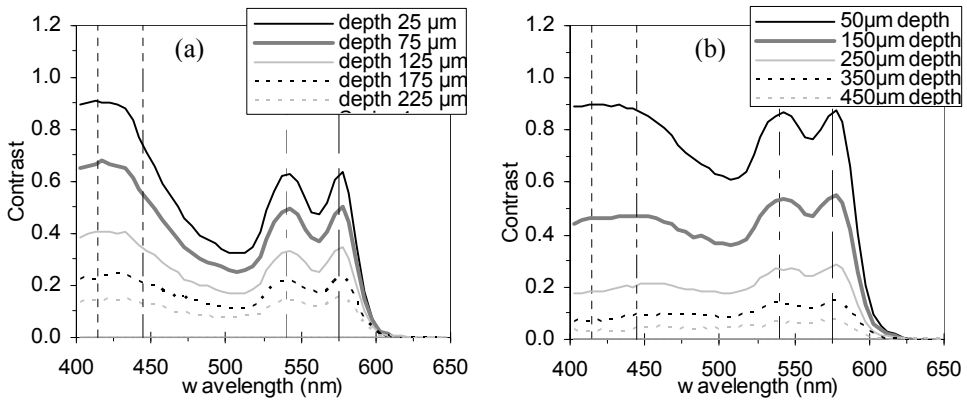

Fig. 8 Contrast as a function of wavelength at different vessel depths for vessel diameters of (a) 50 μm, (b) 100 μm

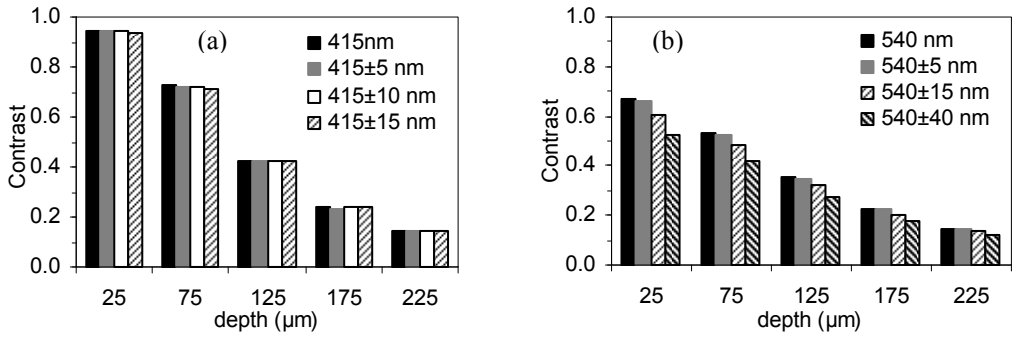

Fig. 9 Contrast as a function of bandwidth and vessel depth when vessel diameter is 50μm

4. DISCUSSION AND CONCLUSION

Our study quantitatively shows that 415±15 nm band produced higher contrast than 540±10 nm band for smaller vessels at shallower depth. The reverse was true for larger vessels at deeper region. This phenomenon agreed with Gono *et al*.'s NBI studies on human tongue [13]. They show that the contrast of small vasculature patterns in superficial layers reach a maximum at 415 nm while contrast of large vasculature patterns at deeper region are optimal at 540 nm and 575 nm wavelengths [13]. While these studies explained the basic effects of Hb absorption and tissue scattering, they did not quantify the effect of vessel depth on contrast and didn't specify the location of imaged vessels. The overall superior contrast of narrow band light to white light shown in our studies (Fig. 6 b,d&e) was comparable to that reported in other NBI studies [6, 32, 33]. However, we also quantified that white light might produce images with higher contrast than the 415±15 nm band for large vessels (diameter 200 μm) at deep region.

Previous studies also mentioned that better contrast could be obtained by using narrower bandwidth, for example 540±10 nm versus 540±40 nm [13]. This was due to the cut off of wavelengths that consisted of smaller Hb absorption [13]. In this study, we established the similar conclusions for 540 nm region as shown in Fig. 9b. For the center wavelength of 415 nm cases, however, our results indicate that increasing bandwidth in certain range did not decrease contrast. In that case, a broader band might be preferred.

NBI contrast was strongly affected by blood vessel depth and diameter, as well as wavelength (Hb absorption and tissue scattering). By showing contrast as a function of vessel depth, vessel size, wavelength and band width based on model simulations, we were able to identify potentially optimal wavelengths for visualizing specific vessel geometries. For example, Fig. 6c suggested that the 415±15 nm band had better contrast than the 540±10 nm band for vessel diameter of 75 μm at depths of less than 125 μm, while the 540±10 nm band provided better visualization for the same vessel size at depths greater than 125 μm. Overall, our study showed that a MC modeling approach can provide novel, quantitative insight into NBI, and may lead to improvements in performance.

Disclaimer: The mention of commercial products, their sources, or their use in connection with material reported herein is not to be construed as either an actual or implied endorsement of such products by the Department of Health and Human Services.

REFERENCES

[1] Siegel, R., Ward, E., Brawley, O., and Jemal, A., "Cancer statistics, 2011," CA. Cancer J. Clin. **61,** 212-236 (2011).

[2] Kumagai, Y., Toi, M., and Inoue, H., "Dynamism of tumour vasculature in the early phase of cancer progression: outcomes from oesophageal cancer research," Lancet Oncol. **3,** 604-610 (2002).

[3] Torres, C., Wang, H., Turner, J., Shahsafaei, A., and Odze, R. D., "Prognostic significance and effect of chemoradiotherapy on microvessel density (angiogenesis) in esophageal Barrett's esophagus-associated adenocarcinoma and squamous cell carcinoma," Human Pathology **30,** 753-758 (1999).

[4] Sharma, P., Bansal, A., Mathur, S., Wani, S., Cherian, R., McGregor, D., Higbee, A., Hall, S., and Weston, A., "The utility of a novel narrow band imaging endoscopy system in patients with Barrett's esophagus," Gastrointest. Endosc. **64,** 167-175 (2006).

[5] Takano, J. H., Yakushiji, T., Kamiyama, I., Nomura, T., Katakura, A., Takano, N., and Shibahara, T., "Detecting early oral cancer: narrowband imaging system observation of the oral mucosa microvasculature," Int. J. Oral Maxillofac. Surg. **39,** 208-213.

[6] Yoshida, T., Inoue, H., Usui, S., Satodate, H., Fukami, N., and Kudo, S., "Narrow-band imaging system with magnifying endoscopy for superficial esophageal lesions," Gastrointest. Endosc. **59,** 288-295 (2004).

[7] Ishihara, R., Inoue, T., Uedo, N., Yamamoto, S., Kawada, N., Tsujii, Y., Kanzaki, H., Hanafusa, M., Hanaoka, N., Takeuchi, Y., Higashino, K., Iishi, H., Tatsuta, M., Tomita, Y., and Ishiguro, S., "Significance of each narrow-band imaging finding in diagnosing squamous mucosal high-grade neoplasia of the esophagus," J. Gastroenterol. Hepatol. **25,** 1410-1415 (2010).

[8] Sharma, P., Wani, S., Bansal, A., Hall, S., Puli, S., Mathur, S., and Rastogi, A., "A feasibility trial of narrow band imaging endoscopy in patients with gastroesophageal reflux disease," Gastroenterology **133,** 454-464 (2007).

[9] Tanaka, S., Hirata, M., Oka, S., Kaneko, I., Yoshida, S., Yoshihara, M., and Chayama, K., "Magnifying endoscopy with narrow band imaging for diagnosis of colorectal tumors," Gastrointest. Endosc. **65,** 988-995 (2007).

[10] Uraoka, T., Saito, Y., Ikematsu, H., Yamamoto, K., and Sano, Y., "Sano's Capillary Pattern Classification for Narrow-Band Imaging of Early Colorectal Lesions," Digestive Endoscopy **23,** 112-115 (2011).

[11] Horimatsu, T., Ikematsu, H., Sano, Y., Katagiri, A., Fu, K. I., Ohtsu, A., and Yoshida, S., "A micro-vascular architecture with NBI colonoscopy is useful to predict invasiveness and allow patients to select for endoscopic resection or surgical resection," Gastrointest. Endosc. **65,** Ab270-Ab270 (2007).

[12] Su, M. Y., Hsu, C. M., Ho, Y. P., Chen, P. C., Lin, C. J., and Chiu, C. T., "Comparative study of conventional colonoscopy, chromoendoscopy, and narrow-band imaging systems in differential diagnosis of neoplastic and nonneoplastic colonic polyps," Am. J. Gastroenterol. **101,** 2711-2716 (2006).
[13] Gono, K., Obi, T., Yamaguchi, M., Ohyama, N., Machida, H., Sano, Y., Yoshida, S., Hamamoto, Y., and Endo, T., "Appearance of enhanced tissue features in narrow-band endoscopic imaging," J. Biomed. Opt. **9,** 568-577 (2004).
[14] Gono, K., Yamazaki, K., Doguchi, N., Nonami, T., Obi, T., Yamaguchi, M., Ohyama, N., Machida, H., Sano, Y., Yoshida, S., Hamamoto, Y., and Endo, T., "Endoscopic observation of tissue by narrowband illumination," Optical Review **10,** 211-215 (2003).
[15] Itoi, T., Sofuni, A., Itokawa, F., Tsuchiya, T., Kurihara, T., Ishii, K., Tsuji, S., Moriyasu, F., and Gotoda, T., "Peroral cholangioscopic diagnosis of biliary-tract diseases by using narrow-band imaging (with videos)," Gastrointest. Endosc. **66,** 730-736 (2007).
[16] Waldner, M. J., Wirtz, S., Neufert, C., Becker, C., and Neurath, M. F., "Confocal laser endomicroscopy and narrow-band imaging-aided endoscopy for in vivo imaging of colitis and colon cancer in mice," Nat. Protoc. **6,** 1471-1481 (2011).
[17] Akbari, H., Kosugi, Y., Kojima, K., Toshiaki Ohya, Akamatsu, H., and Tanaka, N., "Enhanced Blood Vessels in Laparoscopy by Using Narrow-Band Imaging," in *MVA2007 IAPR Conference on Machine Vision Applications*, (Tokyo, Japan, 2007).
[18] Pfefer, T. J., Barton, J. K., Chan, E. K., Ducros, M. G., Sorg, B. S., Milner, T. E., Nelson, J. S., and Welch, A. J., "A three-dimensional modular adaptable grid numerical model for light propagation during laser irradiation of skin tissue," IEEE J. Sel. Top. Quantum Electron. **2,** 934-942 (1996).
[19] Fang, Q. Q., and Boas, D. A., "Monte Carlo Simulation of Photon Migration in 3D Turbid Media Accelerated by Graphics Processing Units," Optics Express **17,** 20178-20190 (2009).
[20] Custo, A., Wells, W. M., Barnett, A. H., Hillman, E. M. C., and Boas, D. A., "Effective scattering coefficient of the cerebral spinal fluid in adult head models for diffuse optical imaging," Appl. Opt. **45,** 4747-4755 (2006).
[21] Drezek, R., Sokolov, K., Utzinger, U., Boiko, I., Malpica, A., Follen, M., and Richards-Kortum, R., "Understanding the contributions of NADH and collagen to cervical tissue fluorescence spectra: Modeling, measurements, and implications," J. Biomed. Opt. **6,** 385-396 (2001).
[22] Chang, S. K., Arifler, D., Drezek, R., Follen, M., and Richards-Kortum, R., "Analytical model to describe fluorescence spectra of normal and preneoplastic epithelial tissue: comparison with Monte Carlo simulations and clinical measurements," J. Biomed. Opt. **9,** 511-522 (2004).
[23] Friebel, M., Roggan, A., Muller, G., and Meinke, M., "Determination of optical properties of human blood in the spectral range 250 to 1100 nm using Monte Carlo simulations with hematocrit-dependent effective scattering phase function," J. Biomed. Opt. **11,** - (2006).
[24] Beutler, E., and Waalen, J., "The definition of anemia: what is the lower limit of normal of the blood hemoglobin concentration?," Blood **107,** 1747-1750 (2006).
[25] Greenberg, G., Assali, A., Vaknin-Assa, H., Brosh, D., Teplitsky, I., Fuchs, S., Battler, A., Kornowski, R., and Lev, E. I., "Hematocrit Level as a Marker of Outcome in ST-Segment Elevation Myocardial Infarction," Am. J. Cardiol. **105,** 435-440 (2010).
[26] Faber, D. J., Aalders, M. C. G., Mik, E. G., Hooper, B. A., van Gemert, M. J. C., and van Leeuwen, T. G., "Oxygen saturation-dependent absorption and scattering of blood," Phys. Rev. Lett. **93,** 028102 (2004).
[27] Puvanakrishnan, P., Park, J., Diagaradjane, P., Schwartz, J. A., Coleman, C. L., Gill-Sharp, K. L., Sang, K. L., Payne, J. D., Krishnan, S., and Tunnell, J. W., "Near-infrared narrow-band imaging of gold/silica nanoshells in tumors," J. Biomed. Opt. **14,** (2009).
[28] Kuznetsov, K., Lambert, R., and Rey, J. F., "Narrow-band imaging: Potential and limitations," Endoscopy **38,** 76-81 (2006).
[29] Mizuno, H., Gono, K., Takehana, S., Nonami, T., and Nakamura, K., "Narrow Band Imaging Technique," *Techniques in Gastrointestinal Endoscopy* **5,** 78-81 (2003).
[30] Shibuya, K., Hoshino, H., Chiyo, M., Iyoda, A., Yoshida, S., Sekine, Y., Iizasa, T., Saitoh, Y., Baba, M., Hiroshima, K., Ohwada, H., and Fujisawa, T., "High magnification bronchovideoscopy combined with narrow band imaging could detect capillary loops of angiogenic squamous dysplasia in heavy smokers at high risk for lung cancer," Thorax **58,** 989-995 (2003).
[31] Takano, J. H., Yakushiji, T., Kamiyama, I., Nomura, T., Katakura, A., Takano, N., and Shibahara, T., "Detecting early oral cancer: narrowband imaging system observation of the oral mucosa microvasculature," Int. J. Oral Maxillofac. Surg. **39,** 208-213 (2010).
[32] Ezoe, Y., Muto, M., Horimatsu, T., Minashi, K., Yano, T., Sano, Y., Chiba, T., and Ohtsu, A., "Magnifying narrow-band imaging versus magnifying white-light imaging for the differential diagnosis of gastric small depressive lesions: a prospective study," Gastrointest. Endosc. **71,** 477-484 (2010).
[33] Chiu, H. M., Chang, C. Y., Chen, C. C., Lee, Y. C., Wu, M. S., Lin, J. T., Shun, C. T., and Wang, H. P., "A prospective comparative study of narrow-band imaging, chromoendoscopy, and conventional colonoscopy in the diagnosis of colorectal neoplasia," Gut **56,** 373-379 (2007).